# Wireless Power Hotspot that Charges All of Your Devices

Lixin Shi, Zachary Kabelac, Dina Katabi, David Perreault
Massachusetts Institute of Technology
Cambridge, MA, USA
{lixin, zek, dina}@csail.mit.edu, djperrea@mit.edu

## ABSTRACT

Each year, consumers carry an increasing number of gadgets on their person: mobile phones, tablets, smartwatches, etc. As a result, users must remember to recharge each device, every day. Wireless charging promises to free users from this burden, allowing devices to remain permanently unplugged. Today's wireless charging, however, is either limited to a single device, or is highly cumbersome, requiring the user to remove all of her wearable and handheld gadgets and place them on a charging pad.

This paper introduces MultiSpot, a new wireless charging technology that can charge multiple devices, even as the user is wearing them or carrying them in her pocket. A MultiSpot charger acts as an access point for wireless power. When a user enters the vicinity of the MultiSpot charger, all of her gadgets start to charge automatically. We have prototyped MultiSpot and evaluated it using off-the-shelf mobile phones, smartwatches, and tablets. Our results show that MultiSpot can charge 6 devices at distances of up to 50 cm.

## CATEGORIES AND SUBJECT DESCRIPTORS

C.2.2 [**Computer Systems Organization**]: Computer-Communications Networks

## KEYWORDS

Wireless Power Transfer; MIMO; Magnetic Resonance; Energy; Beamforming; Mobile and Wearable Devices

## 1. INTRODUCTION

Our daily lives rely on a multitude of personal mobile devices, such as phones, tablets, and wearables. While every new device has made our lives easier in many respects, having to remember and manage to charge all of our mobile devices is a recurring and increasingly significant burden. If we could wirelessly charge our devices, it would alleviate this daily anxiety, and may even allow such devices to be permanently unplugged. While previous work has taken initial steps towards this goal, it remains limited to a single device at a time [1, 2, 3], or is highly cumbersome requiring the user to remove all of her wearable and handheld gadgets and place them on a charging pad [4, 5], as in Fig. 1a.


*MobiCom'15,* September 07–11, 2015, Paris, France.

DOI: http://dx.doi.org/10.1145/2789168.2790092.

Imagine, however, if one had a single wireless charger that was able to charge all of its surrounding devices simultaneously, even if they were on the user's body or in her purse. In some sense, this would emulate a miniature WiFi hotspot –i.e., the wireless charger would act as a power access point; once the user is in the vicinity of the charger, her devices start receiving power as needed, and if she moves away the charging stops. One could use such a charger as a desk mat. Whenever the user sits at her desk, the iPhone in her pocket, the tablet in her purse, and the smartwatch on her wrist would charge automatically without even thinking of them, as shown in Fig. 1b.

But how can one deliver a wireless power hotspot? As we investigate the answer to this question, we focus on charging via magnetic coupling because it is the approach adopted by the wireless charging standards [6, 7] and all consumer wireless charging products, and is deemed safe and compliant with FCC rules [8].[1] In magnetic coupling, the power transmitter uses one or more coils. When an AC current traverses the transmitter's coil, it creates a variable magnetic field. If this magnetic field traverses a nearby coil, it generates an electric current, hence delivering power to that device. The stronger the magnetic field is at the receiver, the more power is delivered. The challenge, however, is that the magnetic field dies very quickly with distance, and hence typical wireless charging devices operate at a very short distance of a couple of centimeters [6, 15].

Last year however, a MobiCom paper proposed a solution called MagMIMO [1], where multiple coils on the transmitter act as a multi-antenna system, shaping the magnetic field in a beam and focusing it on the receiver, in a manner similar to beamforming in MIMO systems.[2] The paper demonstrated that for *a single receiver*, beamforming of the magnetic field can increase the charging range up to 40 cm and allow for a flexible phone orientation. Motivated by this recent development, we investigate whether one can charge multiple receivers at distance by shaping the magnetic field in multiple beams focused on the various receivers.

At first blush, it might seem that one can beamform the magnetic field to multiple receivers by directly borrowing from multi-user MIMO. Unfortunately, there is an intrinsic difference between multi-user MIMO in RF communications and the physics of wireless charging. Specifically, consider the effect of introducing mul-

[1] In particular, we use magnetic resonance [7]. Some start-ups have advocated the use of RF radiation [9, 10], ultrasound [11], or lasers [12] for wireless power transfer. None of those approaches have made it into the standards for consumer electronics. Further, charging consumer electronics, e.g., phones, using RF or lasers raises safety concerns [13, 14] (for further details see §2).

[2] The term "magnetic beamforming" in [1] and this paper refers to shaping the magnetic flux in the near field in the form of a beam (or multiple beams). In contrast, traditional beamforming in wireless communication systems operates over radiated waves in the far field.


(a) Today's Wireless Charging (b) MultiSpot Charging Hotspot

Figure 1: (a): Today's wireless chargers require careful placement of each device on the charging pad. (b) MultiSpot acts as a wireless power hotspot. Mounted as a desk mat, it charges all surrounding personal electronics, including cellphones, tablets, smartwatches, wireless keyboards and touchpads.

tiple receivers. In a conventional wireless communication system, each receiver is a passive listener that only receives signals. In contrast, in a wireless charging system, receivers interact with each other. A receiver not only accepts power, but also reflects power back to the transmitters and other receivers. The presence of a receiver affects the magnetic field observed by other receivers and transmitters. As a result, adding, removing, or moving just a single receiver in the system affects all of the other receivers, which is not the case in RF communication systems. In fact not accounting for these interactions can lead to large errors in shaping the magnetic field and consequent charging failures, as we show in §7.2. One therefore needs to account for these fundamental differences between the models of multi-user RF channels and multi-receiver magnetic channels, while formulating and solving the magnetic charging problem.

This paper introduces MultiSpot, a multi-coil power transmitter that can beam its magnetic field toward multiple power receivers simultaneously. MultiSpot formulates the multi-receiver magnetic charging problem and derives a solution whose equations account for inter-receiver interactions. By shaping the magnetic field into beams and focusing them towards the receivers, MultiSpot can significantly increase the range of multi-receiver wireless charging. Further, by steering the beams with receiver motion and orientation, MultiSpot can accommodate a flexible charging pattern capable of charging a smartwatch on the user's wrist, a phone in her hand, and a tablet in her purse.

MultiSpot has three key features:

1. MultiSpot is analytically proven to maximize the power delivered to the receivers. Said differently, given an input power and a particular topology of the transmit and receive coils (and hence their resulting magnetic couplings), MultiSpot delivers a closed-form solution that sets the charging parameters to guarantee maximum power delivery to the receivers' coils.
2. MultiSpot's solution is adaptive. It adjusts to movements of the receivers and re-converges to the optimal solution. In our implementation, MultiSpot adapts to receivers' movements in just a few milliseconds.
3. A MultiSpot charger can beamform without any communication or coordination of the receivers, despite the fact that MultiSpot's beamforming is impacted by the interactions between the receivers (i.e., their inter-receiver magnetic couplings). The MultiSpot transmitter passively infers all needed information based on the reflected power it observes at the Tx coils.

**Implementation and Results:** We built a prototype of MultiSpot and evaluated it with smart phones, a smartwatch, and a tablet. We also compared MultiSpot to multiple baselines: Duracell Powermat [4], Energizer Qi [5] and LUXA2 [16], and a reference design by WiTricity called WiT-5000 [15]. Our results show the following:

- MultiSpot can charge 6 devices at distances up to 50 cm, whereas the baselines are limited to 2 devices at 5cm.
- MultiSpot charges different types of devices simultaneously. When attached to an office desk, and with the user sitting at the desk, MultiSpot simultaneously charged a smartwatch on the user's wrist, an iPhone in her pocket, and a nearby tablet, keyboard, and touchpad.
- MultiSpot's charging time is lower than all wireless charging baselines, for the same distance. The charging time depends on distance. For distances less than 20 cm, MultiSpot charges two phones from dead batteries to full charge in less than 1.5x of the time taken for wired charging. The charging time increases to 3x when the phones are 35cm away from the charger, and 5x when they are 50cm away.
- Interestingly, the presence of multiple receivers can increase the range of power transfer. We show that the maximal range is 10cm larger with two phones than it is with one phone, and 17cm larger with 4 phones.
- Finally, we compare MagMIMO [1] to MultiSpot in the presence of two phones. Our results show that MagMIMO's charging time is comparable to MultiSpot *only* when the two phones are co-located and hence can be considered as one device. Otherwise, MagMIMO takes an order of magnitude longer time or might fail to charge one of the phones altogether. This is because MagMIMO has no mechanism to disentangle the magnetic couplings of different receivers, and hence in the presence of multiple receivers it can fail to compute the correct beamforming solution.

**Contributions:** 1) A provably optimal solution to maximize power transfer to multiple receivers by shaping the magnetic field of a multi-coil power transmitter. 2) An implementation and empirical evaluation with off-the-shelf devices including smart phones, a smart watch, and a tablet. 3) Empirical results showing that MultiSpot's magnetic coupling can charge mobile phones and wearables up to 50 cm and in flexible orientations.

## 2. Related Work

Wireless power transfer has spread across a vast array of fields expanding the capabilities of devices such as phones [4, 17], wearables [18], medical implants [19, 20], electric vehicles [21], sensors [22, 23], etc.

The standard approach for wireless charging of consumer devices is based on magnetic coupling. In fact, magnetic coupling is used in all commercial wireless chargers for phones and smartwatches [3, 24], as well as current industry standards [6, 7]. Earlier products have used inductive magnetic coupling [17], but recent ones are moving to magnetic resonance, which yields higher efficiency [25]. Commercial chargers however are highly limited in both range and flexibility. They require the user to carefully place her charged devices on the charging pad and have them perfectly aligned with the pad [4, 5, 16], as in Fig.1a.

Academic research has taken important steps towards wirelessly delivering power to multiple receivers using magnetic coupling. We distinguish between two classes of work: The first class can deal with a small receiver coil that fits in the back of a phone or the strap of a smartwatch and achieve a maximum distance of 10 cm [26, 27, 28, 29]. The second class can deliver power at larger ranges up to 30cm [30, 31, 32], but they require large receiver coils that could

not possibly fit on the back of a phone or wearable. In addition, both classes assume the receiver coil is aligned with the transmitter coil, and do not deal with different receiver orientations with respect to the transmitter. In practice, however, the user cannot benefit from an increase in charging distance if she has to hold her device on top of the charging pad and maintain a perfect alignment with the charger. MultiSpot is unique in that it adapts the shape of the magnetic field according to the location and orientation of the receivers by constructively combining the magnetic fields of multiple Tx coils. This allows MultiSpot to reduce the size of the receiver coil to fit on phones and wearables, while supporting larger ranges and flexible receiver orientations.

Researchers have also explored using multiple transmit coils to beamform the magnetic field to receivers. In fact, MultiSpot is inspired by MagMIMO's techniques [1]. However, as described earlier in Sec. §1, MagMIMO does not work in the presence of more than one receiver, while MultiSpot is designed to work with any number of receivers. We show in experiments (Sec.§7) that when two receivers are separated from each other, MagMIMO cannot charge them.

Very recently, another work was accepted for publication, which also uses multiple transmit coils, and examines the possibility of combining their fields at up to 2 receivers [33]. While the work demonstrates the potential of multi-user charging, it presents an optimal solution only for a single receiver, and uses brute force exploration to determine the optimal solution for two receivers. Further, the work presents an implementation only for the single receiver case, and uses simulation for the two-receiver case. In contrast, MultiSpot presents an optimal solution for any number of receivers. Further, MultiSpot is implemented and empirically evaluated for up to 6 receivers.

We also note that there have been recent proposals of wireless charging using physical phenomena other than magnetic coupling. Ultrasound [11], lasers [12], and power delivery via RF radiation [9, 10] have been proposed by startup companies. However, none of these companies have published their technologies nor offered a product. Furthermore, ultrasound charging is limited to line-of-sight scenarios and will be disrupted if the phone is not directly in front of the charger [34]. It can also negatively affect pets who hear some types of ultrasound [35]. Lasers can cause damage to one's eyesight [13], and delivering power to mobile devices via RF radiation at hundreds of MHz to GHz heats up water which composes most of a human body, similarly to how a microwave oven cooks food [14].[3] Beyond the safety problems, it is also unclear how these technologies can be compliant with FCC regulations.

## 3. PRIMER

In this section, we explain how magnetic coupling works at a high level. In this approach, the transmitter coil is driven by an AC current to generate an oscillating magnetic field. When another conductive coil is placed within range of the transmitter, some of the magnetic field passes through the center of its coil. This field induces an AC current on the receiver, which can be used to power the device.

To boost the efficiency of power transfer, state-of-the-art systems and industrial standards [6, 7], use a technique called *magnetic resonance* [25], in which they add a capacitor to the transmitter and receiver circuits and make them resonate at the same frequency. The oscillations cause the circuits to resonate back and forth without consuming much energy. Magnetic resonance is the underlying power transfer mechanism used in MultiSpot.

[3]To see how delivering power via RF radiation to a phone might be dangerous, let us do a rough calculation. Say that a standard phone requires at least 1W to turn on charging, and it has an area of 5cm×10cm, i.e., the power density is 20mW/cm$^2$. As a comparison, FDA (Food and Drug Administration) enforces microwave oven leakage to be below 5mW/cm$^2$ in order to be considered safe [36].

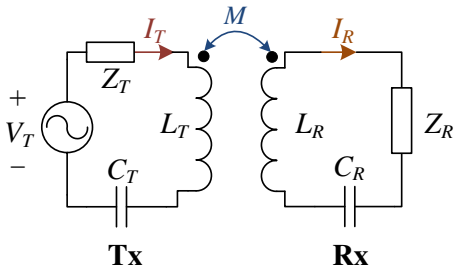


Figure 2: **Single-Coil Tx, Single Rx Schematic**

### 3.1 Circuit Equations

Magnetic coupling and the resulting power transfer can be mathematically described via basic circuit equations [37].

**Single Coil System:** Consider the system in Fig. 2, which shows a single coil transmitter and a single receiver. Let us write the equations that describe this system. As we do so, we will take into account that in magnetic resonance, the inductance and capacitor are chosen so that their impacts cancel each other at the resonant frequency (i.e., $j\omega L + \frac{1}{j\omega C} = 0$). Thus, we can ignore those terms.

We can describe the system in Fig. 2 using two equations. The first equation determines how a current in the transmit coil, $I_T$, induces a current in the receive coil, $I_R$, i.e.:

$$Z_R I_R = j\omega M I_T \tag{1}$$

where $M$ is the magnetic coupling between the transmit and receive coils, $Z_R$ is the impedance of the receiver and $\omega$ is the resonant frequency.

The above equation would have been sufficient to describe the system if one could directly apply a current to the transmit coil. Unfortunately, in practice, one has to use a voltage source instead. Thus, we need a second equation that determines the relationship between the voltage one applies to the transmitter, $V_T$ and the resulting transmitter current, $I_T$.

For the circuit in Fig. 2, we have: $V_T = Z_T I_T - j\omega M I_R$, where $Z_T$ represents the impedance in the transmitter. Note in this equation how the current in the receiver induces a voltage back on the transmitter via the same magnetic coupling $M$. We can further substitute $I_R$ from Eq. (1) to obtain:

$$V_T = \left(Z_T + \omega^2 M^2 / Z_R\right) I_T. \tag{2}$$

Together Eq. (1) and Eq. (2) describe the single-coil charging system.

**Multi-Coil System:** The above two equations can be generalized to the case of multiple transmitter coils and multiple receiver coils, shown in Fig. 3a. The difference is that now every pair of coils has magnetic coupling between them. Specifically, there are three types of couplings: $M_{Tik}$ between transmitter $i$ and $k$, $M_{iu}$ between transmitter $i$ and receiver $u$, and $M_{Ruv}$ between receiver $u$ and $v$.

We can update Eq. (1) and Eq. (2) to account for the additional coupling between transmitter coils, and between receiver coils. Re-

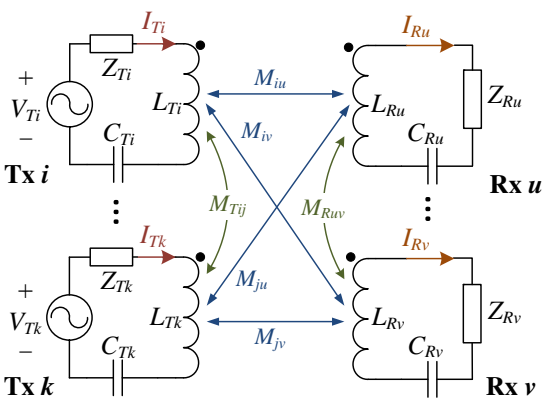


(a) Multi-coil Tx, Multiple Rx Schematic

| Term | Definition | Explanation |
|---|---|---|
| $n$ | Number of Tx coils | |
| $m$ | Number of Rx coils | |
| $\vec{\boldsymbol{v}}_T$ | $[V_{T1}, V_{T2}, \cdots, V_{Tn}]^\top_{n\times 1}$ | Tx voltages |
| $\vec{\boldsymbol{i}}_T$ | $[I_{T1}, I_{T2}, \cdots, I_{Tn}]^\top_{n\times 1}$ | Tx currents |
| $\vec{\boldsymbol{i}}_R$ | $[I_{R1}, I_{R2}, \cdots, I_{Rm}]^\top_{n\times 1}$ | Rx currents |
| $\boldsymbol{Z}_R$ | $\begin{bmatrix} Z_{R1} & j\omega M_{R12} & \cdots & j\omega M_{R1m} \\ j\omega M_{R21} & Z_{R2} & \cdots & j\omega M_{R2m} \\ \vdots & \vdots & \ddots & \vdots \\ j\omega M_{Rm1} & j\omega M_{Rm2} & \cdots & Z_{Rm} \end{bmatrix}_{m\times m}$ | Rx impedance and inter-Rx magnetic couplings |
| $\boldsymbol{Z}_T$ | $\begin{bmatrix} Z_{T1} & j\omega M_{T12} & \cdots & j\omega M_{T1n} \\ j\omega M_{T21} & Z_{T2} & \cdots & j\omega M_{T2n} \\ \vdots & \vdots & \ddots & \vdots \\ j\omega M_{Tn1} & j\omega M_{Tn2} & \cdots & Z_{Tn} \end{bmatrix}_{n\times n}$ | Tx impedance and inter-Tx magnetic couplings |
| $\boldsymbol{M}$ | $\begin{bmatrix} M_{11} & M_{21} & \cdots & M_{n1} \\ \vdots & \vdots & \ddots & \vdots \\ M_{1m} & M_{2m} & \cdots & M_{nm} \end{bmatrix}_{m\times n}$ | Tx-Rx magnetic couplings |

(b) Matrix & Vector Denotations

Figure 3: **Circuit Schematic and Denotations of a Multi-Coil Tx, Multiple Rx Wireless Power Delivery System**

ceiver $u$'s circuit equation becomes:

$$Z_{Ru}I_{Ru} + \underbrace{\sum_{v\neq u} j\omega M_{Ruv}I_{Rv}}_{\text{from the other receivers}} = \underbrace{\sum_{i} j\omega M_{iu}I_{Ti}}_{\text{from the transmitters}} \quad (3)$$

while the transmitter voltage at coil $i$ is:

$$V_{Ti} = Z_{Ti}I_{Ti} + \underbrace{\sum_{k\neq i} j\omega M_{Tik}I_{Tk}}_{\text{from the other transmitters}} - \underbrace{\sum_{u} j\omega M_{iu}I_{Ru}}_{\text{from the receivers}} \quad (4)$$

For convenience, we rewrite Eq. (3) and (4) in matrix form:

$$\text{Rx Equation:} \quad \vec{\boldsymbol{i}}_R = j\omega \boldsymbol{Z}_R^{-1}\boldsymbol{M}\vec{\boldsymbol{i}}_T \quad (5)$$

$$\text{Tx Equation:} \quad \vec{\boldsymbol{v}}_T = \left(\boldsymbol{Z}_T + \omega^2 \boldsymbol{M}^\top \boldsymbol{Z}_R^{-1}\boldsymbol{M}\right)\vec{\boldsymbol{i}}_T \quad (6)$$

where the matrix and vector denotations are defined in Table 3b.[4]

Eq. (5) and Eq. (6) are sufficient to describe the multi-coil system in Fig. 3a. Specifically, Eq. (5) describes what receiver current $\vec{\boldsymbol{i}}_R$ we will get if a transmitter current $\vec{\boldsymbol{i}}_T$ is applied, thus we call it the *Receiver Equation*. Eq. (6), on the other hand, shows what voltage $\vec{\boldsymbol{v}}_T$ we need to apply in order to obtain transmitter currents $\vec{\boldsymbol{i}}_T$, so we name it the *Transmit Equation*. These two equations describe the most fundamental relationships in our multi-Tx multi-Rx system, and are the basis of *all* of the following conclusions of MultiSpot.

## 4. MULTISPOT

MultiSpot is a new technology for charging multiple devices wirelessly via magnetic resonance. It uses multiple transmit coils, which could be built into a desk mat to deliver a user experience analogous to a mini hotspot –i.e., when the user sits at her desk, all of her electronic gadgets start receiving power automatically. MultiSpot's design is mainly focused on the transmitter side. The receiver design follows that of standard wireless charging circuits, which can be built into the sleeve of a phone or the strap of a smartwatch.

[4]Note that similar to the single-Tx single-Rx case, Eq. (6) is obtained by first rewriting Eq. (4) into $\vec{\boldsymbol{v}}_T = \boldsymbol{Z}_T\vec{\boldsymbol{i}}_T - j\omega\boldsymbol{M}^\top\vec{\boldsymbol{i}}_R$ and then substituting $\vec{\boldsymbol{i}}_R$ using Eq. (5).

At first blush, it might seem that one can build a wireless power hotspot by beamforming the magnetic field to one receiver at a time using MagMIMO [1], and iterating between receivers using a TDMA style MAC. Unfortunately MagMIMO intrinsically assumes only one receiver. If multiple receivers are nearby, they all couple with each other and the transmitter coils. As a result, MagMIMO cannot discover the coupling due to each receiver (i.e., the magnetic channel to the receiver [1]) and hence cannot compute the beamforming parameters correctly. In fact MagMIMO would not know whether there is a single or multiple receivers. One could also try to add out-of-band communication (via WiFi or Bluetooth) to coordinate receivers, turn some receivers off so that at any point in time there is coupling only from one receiver, synchronize the receivers as they turn on and off, and have receivers detect any motion and inform each other so that they may re-estimate coupling. Such an approach is excessively complex and high overhead, and is not even clear how one can extend this idea into a full system.

Below we describe a design that requires neither receiver coordination nor out-of-band communication. It operates entirely on the transmitter allowing it to shape the magnetic field in multiple beams focused on the receivers, in a manner that is analytically proven to maximize power delivery.

### 4.1 Optimizing Power Delivery to Receivers

In wireless communication systems, such as MU-MIMO, beamforming effectively combines the signals constructively at the receivers so that the received signal gets maximized. This is achieved by carefully setting the transmitter signal according to the wireless channels. Similar concepts can be applied to wireless power delivery systems. However, to beamform in MultiSpot, we need to answer two questions. What exactly are the "signals" and "channels"? And how do we maximize the power of the received signal?

**(a) Magnetic Channel:** The Receiver Eq. (5) provides us a way to analogously define magnetic channels. Specifically, if we analogize currents to signals, the transmitted and received signals will be $\vec{\boldsymbol{i}}_T$ and $\vec{\boldsymbol{i}}_R$. Therefore, the coefficient between them is the magnetic channel, i.e.:

$$\vec{\boldsymbol{i}}_R = \boldsymbol{H}\vec{\boldsymbol{i}}_T, \quad \text{where } \boldsymbol{H} = j\omega\boldsymbol{Z}_R^{-1}\boldsymbol{M} \quad (7)$$

Note that the magnetic channel $\boldsymbol{H}$ is different from the channel matrix in MU-MIMO, where it is simply a concatenation of in-

dividual channels between every pair of transmitter and receiver. Rather, in MultiSpot, it is the multiplication of two parts: $\boldsymbol{H} = \boldsymbol{H}_{Rx-Rx}\boldsymbol{H}_{Rx-Tx}$ where $\boldsymbol{H}_{Rx-Rx} = \boldsymbol{Z}_R^{-1}$ contains receiver-receiver couplings and $\boldsymbol{H}_{Rx-Tx} = j\omega\boldsymbol{M}$ contains transmitter-receiver couplings. Physically, these two sub-channel matrices describe two processes that occur in multi-TX-coil multi-receiver power transfer system: $\boldsymbol{H}_{Rx-Tx}$ characterizes the induced power on the receivers from transmitters, while $\boldsymbol{H}_{Rx-Rx}$ captures the redistribution of transmitted power among receivers due to receiver-receiver coupling.

**(b) Maximizing Received Power:** The challenge becomes how to set the transmitter signals, (i.e., $\vec{\boldsymbol{i}}_T$), so that the received power is maximized. This question can be formulated as an optimization problem that maximizes the received power $P_R$, under the constraint of a total input power $P$.

The received power $P_R$ can be written as the summation of the power delivered to each receiver, i.e.:

$$P_R = \vec{\boldsymbol{i}}_R^* \boldsymbol{R}_R \vec{\boldsymbol{i}}_R, \tag{8}$$

where $\vec{\boldsymbol{i}}_R$ is a vector of the receiver currents. The superscript $(^*)$ denotes conjugate transpose, and $\boldsymbol{R}_R$ is a diagonal matrix whose entries are the resistances of each receiver.[5]

The input power can be written as the total power dissipated on the transmitter and receivers, i.e., $P = P_R + P_T$. This is because power does not disappear, and hence must either be delivered to the receivers, or be consumed on the transmitters. Thus:

$$P = P_R + P_T = \vec{\boldsymbol{i}}_R^* \boldsymbol{R}_R \vec{\boldsymbol{i}}_R + \vec{\boldsymbol{i}}_T^* \boldsymbol{R}_T \vec{\boldsymbol{i}}_T, \tag{9}$$

where $\boldsymbol{R}_R$ and $\boldsymbol{R}_T$ are diagonal matrices of transmitter and receiver resistances.

Now, we can re-write the optimization problem that maximizes power transfer by substituting the received power and the input power by their values from Eq. (8) and Eq. (9). We also substitute the received currents from Eq. (7), $\vec{\boldsymbol{i}}_R = \boldsymbol{H}\vec{\boldsymbol{i}}_T$. Thus, our optimization problem becomes: Find the transmit currents that satisfy:

$$\begin{aligned} \vec{\boldsymbol{i}}_T^{\text{bf}} &= \arg\max \left\{ \vec{\boldsymbol{i}}_T^* \boldsymbol{H}^* \boldsymbol{R}_R \boldsymbol{H} \vec{\boldsymbol{i}}_T \right\} \\ \text{conditioned on: } & \vec{\boldsymbol{i}}_T^* \boldsymbol{R}_T \vec{\boldsymbol{i}}_T + \vec{\boldsymbol{i}}_T^* \boldsymbol{H}^* \boldsymbol{R}_R \boldsymbol{H} \vec{\boldsymbol{i}}_T = P, \end{aligned} \tag{10}$$

where $\vec{\boldsymbol{i}}_T^{\text{bf}}$ denotes the set of currents that beamforms.

In Appendix A, we prove that the solution to this optimization is:

THEOREM 4.1. *The following transmitter current vector will maximize the received power:*

$$\vec{\boldsymbol{i}}_T^{bf} = c \cdot maxeig(\boldsymbol{H}^* \boldsymbol{R}_R \boldsymbol{H}) \tag{11}$$

*where maxeig $(\boldsymbol{H}^* \boldsymbol{R}_R \boldsymbol{H})$ is the eigenvector of $\boldsymbol{H}^* \boldsymbol{R}_R \boldsymbol{H}$ that corresponds to the largest real eigenvalue $\lambda$, and $c$ is a normalization scalar defined in App. A. Specifically, the maximal delivered power is equal to $\frac{\lambda}{\lambda+1}P$.*

This theorem guarantees that MultiSpot maximizes the power delivered from the transmitter coils to the receiver coils. This means that for the same hardware and any given relative locations of transmitter and receiver coils, no other algorithm can deliver more power than what is specified by the theorem.

**(c) Applying the Beamforming Solution:** The solution from Thm. 4.1 would be sufficient if one could directly apply the currents to the coil. However, in practice, one has to use a voltage source instead. Therefore, we need to convert these currents to their corresponding voltages so that they are directly applicable to the Tx coils via standard voltage sources.

Fortunately, the Transmitter Eq. (6) that relates transmitter currents to voltages was derived in §3.1. Specifically, the set of voltages that we need to apply to the Tx coils is:

$$\vec{\boldsymbol{v}}_T^{\text{bf}} = \left( \boldsymbol{Z}_T + \omega^2 \boldsymbol{M}^\top \boldsymbol{Z}_R^{-1} \boldsymbol{M} \right) \vec{\boldsymbol{i}}_T^{\text{bf}}. \tag{12}$$

In summary, maximizing power delivery requires two steps:

1. Calculate the beamforming currents, $\vec{\boldsymbol{i}}_T^{\text{bf}}$.
2. Convert the currents to voltages by $\vec{\boldsymbol{v}}_T^{\text{bf}}$, and apply the voltages to the transmitter coils.

## 4.2 Eliminating Need for Receivers' Communication

In the previous section, we showed how a MultiSpot charger could beamform. However, two steps are needed to beamform, both of which require information that resides on the receivers, and is unavailable at the transmitter.

- In the first step, the beamforming currents, $\vec{\boldsymbol{i}}_T^{\text{bf}}$, are calculated via Thm. 4.1, which is strictly dependent on knowing $\boldsymbol{H}^* \boldsymbol{R}_R \boldsymbol{H}$. Recall, however, that the channel contains receiver-receiver couplings, unknown to the transmitter.
- In the second step, the beamforming voltages, $\vec{\boldsymbol{v}}_T^{\text{bf}}$, are computed using Eq. (12), which depends on knowing $(\boldsymbol{Z}_T + \omega^2 \boldsymbol{M}^\top \boldsymbol{Z}_R^{-1} \boldsymbol{M})$. $\boldsymbol{Z}_T$ contains only transmitter specific parameters (i.e., transmitter to transmitter couplings and impedances) and hence can be estimated a priori in a factory setting (for details, see Appendix D). However, the matrix $(\omega^2 \boldsymbol{M}^\top \boldsymbol{Z}_R^{-1} \boldsymbol{M})$ contains receiver-receiver couplings and receiver impedances. This matrix which we denote $\boldsymbol{Y} = \omega^2 \boldsymbol{M}^\top \boldsymbol{Z}_R^{-1} \boldsymbol{M}$ is unknown a priori to the transmitter (and changes with time because the coupling depends on receiver position).

Thus, beamforming requires estimating $\boldsymbol{H}^* \boldsymbol{R}_R \boldsymbol{H}$ and $\boldsymbol{Y}$, both of which involve receiver dependent information. So, how can a MultiSpot transmitter estimate these matrices without explicit information from the receivers?

**Estimating $\boldsymbol{Y}$:** Let us first consider estimating $\boldsymbol{Y}$. The Transmitter Eq. (6) can be rewritten as $\vec{\boldsymbol{v}}_T = (\boldsymbol{Z}_T + \boldsymbol{Y})\vec{\boldsymbol{i}}_T$, where the only unknown coefficient is $\boldsymbol{Y}$ because $\boldsymbol{Z}_T$ is measured during pre-calibration. By applying voltages and measuring the resulting currents on the Tx coils, we can estimate the coefficient between them. Since both $\vec{\boldsymbol{v}}_T$ and $\vec{\boldsymbol{i}}_T$ are vectors of length $n$, we need to repeat the measurement process $n$ times before applying matrix inversion, where $n$ is the number of Tx coils. More formally, if one applies $n$ different sets of voltages $\vec{\boldsymbol{v}}_T^{(1)}, \cdots, \vec{\boldsymbol{v}}_T^{(n)}$ and measures the corresponding currents $\vec{\boldsymbol{i}}_T^{(1)}, \cdots, \vec{\boldsymbol{i}}_T^{(n)}$, one can estimate $\boldsymbol{Y}$ by:

$$\boldsymbol{Y} = \left[ \vec{\boldsymbol{v}}_T^{(1)} \ \cdots \ \vec{\boldsymbol{v}}_T^{(n)} \right] \cdot \left[ \vec{\boldsymbol{i}}_T^{(1)} \ \cdots \ \vec{\boldsymbol{i}}_T^{(n)} \right]^{-1} - \ \boldsymbol{Z}_T \tag{13}$$

**Estimating $\boldsymbol{H}^* \boldsymbol{R}_R \boldsymbol{H}$:** After obtaining $\boldsymbol{Y}$, we are still left with the problem of estimating $\boldsymbol{H}^* \boldsymbol{R}_R \boldsymbol{H}$. Recall that $\boldsymbol{H} = j\omega \boldsymbol{Z}_R^{-1} \boldsymbol{M}$, which means both transmitter-receiver couplings and receiver-receiver couplings need to be estimated. Unlike the matrix $\boldsymbol{Y}$ however, which can be estimated at the transmitter using measurements of $\vec{\boldsymbol{v}}_t$ and $\vec{\boldsymbol{i}}_T$, there is no way to measure $\boldsymbol{H}$ at the transmitter.

Fortunately, MultiSpot does not need to estimate $\boldsymbol{H}$. Instead, we show that a MultiSpot transmitter can estimate the matrix product

[5] If a receiver is not fully resistive, i.e., its impedance $Z_{Ru}$ has an imaginary component, then $R_{Ru} = Real(Z_{Ru})$.

**1 MultiSpot Algorithm**

1: $\widetilde{\boldsymbol{Y}} \leftarrow \text{rand}(n \times n)$ ▷$\widetilde{\boldsymbol{Y}}$ can be initialized to any matrix
2: **while** true **do**
3: $\vec{\boldsymbol{i}}_T^{\text{bf}} = c \cdot \text{maxeig}(\text{Real}(\widetilde{\boldsymbol{Y}}))$ ▷compute beamforming currents
4: Apply $\vec{\boldsymbol{v}}_T^{\text{bf}} = \left(\boldsymbol{Z}_T + \widetilde{\boldsymbol{Y}}\right)\vec{\boldsymbol{i}}_T^{\text{bf}}$ ▷beamform
5: Measure $\vec{\boldsymbol{i}}_T$ on the transmitter
6: $\Delta\vec{\boldsymbol{i}}_T \leftarrow \vec{\boldsymbol{i}}_T^{\text{bf}} - \vec{\boldsymbol{i}}_T$
7: **if** $\Delta\vec{\boldsymbol{i}}_T \neq \vec{\boldsymbol{0}}$ **then** ▷ if the channel changes
8: $\widetilde{\boldsymbol{Y}} \leftarrow \widetilde{\boldsymbol{Y}} + \frac{\Delta\vec{\boldsymbol{v}}_T \Delta\vec{\boldsymbol{v}}_T^{\top}}{\Delta\vec{\boldsymbol{v}}_T^{\top}\vec{\boldsymbol{i}}_T}$, where $\Delta\vec{\boldsymbol{v}}_T = (\boldsymbol{Z}_T + \widetilde{\boldsymbol{Y}})\Delta\vec{\boldsymbol{i}}_T$ ▷ update $\widetilde{\boldsymbol{Y}}$
9: **end if**
10: **end while**

$\boldsymbol{H}^*\boldsymbol{R}_R\boldsymbol{H}$ as a whole; and it can do so completely passively. Further, we can relate $\boldsymbol{H}^*\boldsymbol{R}_R\boldsymbol{H}$ to something we have already measured, namely $\boldsymbol{Y}$. Specifically, we prove in Appendix B the following theorem:

THEOREM 4.2. *Define Real$(\cdot)$ as the real part of a matrix, then*

$$\boldsymbol{H}^*\boldsymbol{R}_R\boldsymbol{H} = \textit{Real}(\boldsymbol{Y}) \tag{14}$$

*where* $\boldsymbol{H} = j\omega\boldsymbol{Z}_R^{-1}\boldsymbol{M}$ *and* $\boldsymbol{Y} = \omega^2\boldsymbol{M}^\top\boldsymbol{Z}_R^{-1}\boldsymbol{M}$.

Since we have already shown how to compute $\boldsymbol{Y}$, the above theorem allows us to compute $\boldsymbol{H}^*\boldsymbol{R}_R\boldsymbol{H}$ by taking its real part.

Therefore, we have developed a method to estimate all needed parameters solely on the transmitter, without any communication or feedback from the receivers.

### 4.3 Adaptive Beamforming

Next, we would like to ensure that MultiSpot can smoothly adapt to receiver motion and receivers entering and leaving the system. This is particularly important for wearable receivers which tend to be highly dynamic, e.g., a smartwatch on a user's wrist.

When receivers move (or are added/removed), the magnetic couplings change across all devices, leading to new values for $\boldsymbol{H}$ and $\boldsymbol{Y}$. One could address this problem by repeatedly estimating $\boldsymbol{Y}$ and $\boldsymbol{H}^*\boldsymbol{R}_R\boldsymbol{H}$, as explained in §4.2. This, however, would be suboptimal since estimating $\boldsymbol{Y}$ from scratch requires the MultiSpot charger to stop beamforming and apply other voltages in order to obtain enough measurements as required by Eq. (13). Furthermore, since the transmitter does not know when receivers move, it is left with a difficult choice: Either it can repeat the estimation infrequently, which would be inefficient in scenarios with lots of motion, or it can repeat the estimation, often leading to frequent and unnecessary interruptions in beamforming when the receivers are static.

In this section, we propose an adaptive algorithm, which we call *adaptive beamforming*, that addresses the conflict: It uninterruptedly beamforms whenever the receivers remain static, and seamlessly and quickly adapts when any receiver moves.

The key idea is that instead of estimating $\boldsymbol{Y}$ from scratch, which would interrupt beamforming, the adaptive algorithm iteratively computes the new $\boldsymbol{Y}$. In each iteration, the algorithm computes an incremental update to $\boldsymbol{Y}$ that satisfies the following two constraints: 1) If no receiver moves, the update is zero; and 2) If any receiver moves, the update rule is guaranteed to move $\boldsymbol{Y}$ toward its true value and converge to the true value within a small number of steps.

Alg. 1 outlines MultiSpot's adaptive beamforming. For clarity, we use $\widetilde{\boldsymbol{Y}}$ to denote the algorithm's estimate of the true $\boldsymbol{Y}$ matrix. To start the algorithm randomly assigns an initial matrix to $\widetilde{\boldsymbol{Y}}$. In each iteration, the algorithm calculates the beamforming currents and converts them to beamforming voltages, which it applies to the transmitter coils.

Next (Line 5), the algorithm measures the currents on the transmit coils. If $\widetilde{\boldsymbol{Y}}$ is accurate, the measured currents should be equal to the currents that beamform ($\vec{\boldsymbol{i}}_T^{\text{bf}}$). Otherwise the algorithm uses the mismatch between the measured and expected currents and the resulting mismatch in voltages to update its estimate of $\widetilde{\boldsymbol{Y}}$ (Line 7).

It should be clear from the update rule in Line 7 that if nothing changes (e.g., no receiver moves), no update will occur and the beamforming is unmodified. Further, the theorem below guarantees that when a change occurs, the algorithm quickly converges to the optimal beamforming solution.

THEOREM 4.3. *If $\widetilde{\boldsymbol{Y}} \neq \boldsymbol{Y}$, then Alg. 1 is guaranteed to update $\widetilde{\boldsymbol{Y}}$ to $\boldsymbol{Y}$ in less than $n$ iterations, where $n$ is the number of transmitters.*

Thm. 4.3 is formally proven in Appendix C. Thm. 4.3 not only proves convergence but it puts an upper bound on the time to convergence. The convergence time is bounded only by the number of transmit coils, and is independent of the number of receivers. [6] In our implementation where the transmitter uses a standard microcontroller, each iteration in Alg. 1 can be finished in less than 1ms. When there is any movement, the algorithm takes about 5ms to converge to the new set of channels. This speed is more than sufficient for our application.

### 4.4 Power Distribution Among Receivers

The previous section presents an algorithm that adaptively delivers maximal power to the receivers. But how does the solution distribute this power among the various receivers? In order to gain insight into power distribution, we discuss three representative cases.

- In the first scenario, we consider identical receivers from the perspective of wireless charging – i.e., receivers with the same battery level, distance, and orientation with respect to the transmitter, and hence the same magnetic coupling. In this case, all receivers are allocated equal amounts of power. This is because the system is symmetric with respect to the receivers and hence an even power distribution yields the optimal solution.
- In the second scenario, we consider receivers that have the same battery level (i.e., the same demands for charging), but different magnetic couplings. Physically, this can be caused by some receivers being placed closer to the transmitter than others, with more favorable orientations, or simply having a larger coil. Either way, the receivers with stronger magnetic coupling will receive more power. This property is similar in spirit to resource allocation in typical networking systems. For example, TCP flows with shorter RTTs and WiFi clients with higher SNRs receive higher data rates.
- In the final case, we consider what happens as some receivers approach a fully charged battery while others are still in need for charging. We argue that in this case the MultiSpot charger naturally reduces the power allocated to the more charged receivers, diverting that power to those receivers who are still in need for wireless power. Specifically, consider two receivers with the same magnetic coupling, one of which is fully charged while the other has a low battery level.

[6] It is worth noting that a MultiSpot charger does not need to know the number of receivers to run Alg. 1. The charger has enough information to infer the number of receivers, which is equal to the rank of $\boldsymbol{Y}$.

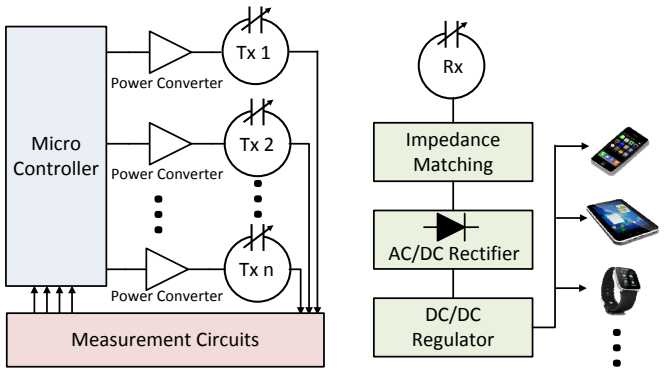


(a) Tx Diagram (b) Rx Diagram

Figure 4: **Circuit Diagram of MultiSpot's Tx and Rx**

When the battery is charged, the device needs very little power so it does not accept current. In this case the receiver circuit can be approximated by an open circuit, i.e., $I_R \approx 0$ for that receiver [38]. As a result, the receiver does not reflect power toward the transmitter. Therefore, the MultiSpot transmitter will not sense this receiver or beamform to it. In general, the progression from accepting current when the receiver has low battery levels to not accepting current when it is fully charged is gradual. Therefore, the algorithm gradually allocates less power to devices that are more charged.

To validate this intuition, we test each of the above situations experimentally in §7.

## 5. IMPLEMENTATION

We have built a prototype of MultiSpot to charge electronics in an office scenario. Our setup is similar to past work [1]. Specifically, the transmitter is composed of 6 copper coils and is mounted to the bottom of an office desk. Each transmit coil covers an area of $0.05\text{m}^2$, which collectively cover an area of $0.38\text{m}^2$. The transmitter can be attached to a regular office desk with metallic, plastic and wood contents. The only restriction of the system is that the desk surface must not be conductive.[7] Each phone receiver contains a single copper coil, of area $0.005\text{m}^2$, that is embedded into a sleeve that attaches to the back of the device. As for the smartwatch, we embed the coil into the band of the watch.

In our implementation, the transmitter and receivers resonate at 1MHz, as in [1], which is within the frequency range of common wireless charging systems [15, 6, 7]. In addition, the setup is compatible with FCC regulations including part 15 and part 18.

The transmitter's architecture is shown in Fig. 4(a). MultiSpot drives 6 transmit coils to beamform a magnetic field towards the receivers. The output voltage and current of each coil are measured by the measurement circuit. This circuit employs quadrature mixers, AD8333 [40], to acquire the phase and amplitude of each signal and output them to the microcontroller. The microcontroller platform, Zynq 7Z010 [41], takes as input these amplitudes and phases and runs MultiSpot's algorithm. Every time Alg. 1 receives new measurements, it updates its estimates accordingly, and calculates the new voltages needed to beamform. It then sends the new set of voltages to the controller circuits which apply them to the transmit coils using a Class D Full Bridge Power Converter [42]. This converter allows the controller circuit to flexibly control both the amplitudes and phases of the voltages applied to the transmit coils.

The receiver circuit is shown in Fig. 4(b). It has an impedance matching network designed to maximize the power that gets delivered to the device. This is followed by a full bridge rectifier which converts the AC signal into a DC voltage. This DC voltage passes through a DC-DC voltage regulator that converts the input voltage to a constant 5V. This allows the power to be distributed across a USB port so that the receiver can support a large variety of unmodified devices that can be charged via USB, including most phones, tablets and wearables.

[7] Conductive materials as large as the desk surface might negatively affect MultiSpot's performance. This is a standard assumption required by magnetic wireless power delivery and can be found in research papers [1] and commercial systems [39].

## 6. EVALUATION ENVIRONMENT

**Metrics:** We define *distance* as the distance between the nearest point on the receiver coil and the transmitter coils. For example, if a receiver is in the same plane of the transmitter but outside the area that the transmitter coils cover, then the distance is from the edge of the receiver to the edge of the nearest transmitter coil.

We define *charging time ratio* as the ratio between the time taken to wirelessly charge a phone from dead to full battery, to the time it takes a wall plug to do the same. For multiple phones, the charging time ratio reported is the largest time ratio of all involved phones, i.e., it is the charging time of the phone that takes longest to charge.

We define *orientation* as the angle between the plane of the receiver coil and the plane of the transmitter coils.

**Baselines:** We compare the following systems:

- Commercially available multi-device wireless chargers: Duracell Powermat [4], Energizer Qi [5] and LUXA2 [16]. Each of them requires a proprietary receiving case, which we attach to the phone during the experiments.
- State-of-the-art Prototype. Specifically, we choose the WiTricity WiT-5000 prototype [15] that charges multiple devices. Since the prototype is not publicly available, we extract the data from their technical sheet [15].
- *Idealized* Selective Coil: This baseline uses the same 6 Tx coils as MultiSpot, but given a set of receivers, it identifies the best Tx coil for each receiver, and divides the input power equally between the set of best Tx coils. For example, given two receivers, it identifies the best Tx coil for the first receiver, and the best Tx coil for the second receiver, and divides the power between those two Tx coils.
  We note that this baseline requires an oracle to decide which Tx coil would deliver the maximum power to each receiver. Specifically, one cannot identify the Tx coil that has the best magnetic coupling to a receiver in the presence of other receivers. Hence, to implement this system, for each receiver, we physically remove the other receivers and measure the receiver coupling to the transmitter. While this is hard to do in a real-world setup, the baseline provides insights about how well one can do by distributing the input power between the best performing Tx coils.
- Our MultiSpot prototype described in §5.
- MagMIMO [1] using the same Tx coils as MultiSpot.

We note that the input powers of Duracell Powermat [4], Energizer Qi [5], LUXA2 [16], and WiTricity WiT-500 [15] are 15W, 18W, 22W, and 24W, respectively. Since these baselines have different input powers, we set the input power of MultiSpot, selective coil, and MagMIMO to the mean of those values, i.e., 20W.

**Setup:** All experiments are performed in an office environment. The charger is placed on a standard office desk. Unless specified otherwise, the charged devices (e.g., phones) are held using config-

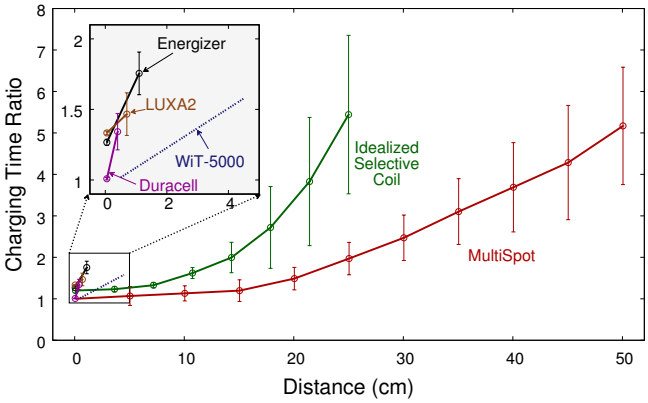


Figure 5: **Charging Time Ratio vs. Distance from Charger.** Each run uses 2 phones at equal distance, but in different locations.

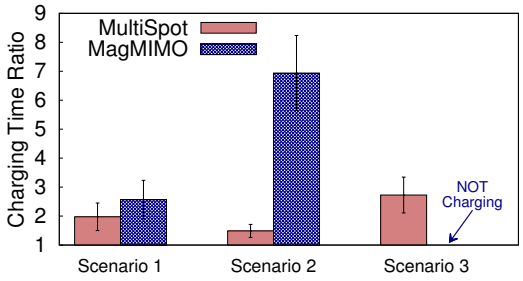


Figure 6: **Comparison with MagMIMO:** Scenario 1: two receivers 5cm apart and both 25cm away from the transmitter; Scenario 2: two receivers 60cm apart and both 10cm away from the transmitter; Scenario 3: two receivers 60cm apart and both 20cm away. The figure shows that MagMIMO works well for co-located receivers, but can completely fail if the receivers are far apart.

urable arms which allows us to test different charging distances and orientations.

## 7. RESULTS

### 7.1 Charging Time vs. Distance

We evaluate MultiSpot's ability to charge multiple phones at various distances from the transmitter. We run each experiment with 2 phones because the commercial baselines are constrained to charging 2 receivers. The distance of both receivers is increased from 2cm to 50cm together. At each distance, multiple experiments are run with different receiver positions and orientations.

Fig. 5 shows the charging time ratio of MultiSpot and the baselines as a function of the distance from the charger. At near distances (0-10cm), MultiSpot's charging time is comparable to a wired charger. It starts to increase at mid-range to far-range. MultiSpot reaches as far as 50cm. Comparing with the baselines, MultiSpot has much larger range, and shorter charging time at the same range. The commercial baselines (Energizer, LUXA2, Duracell) and development prototype (WiT-5000) are constrained to less than 5cm. Even when compared to the idealized selective-coil, MultiSpot reaches much larger range. And even within the same range, MultiSpot's charging time is on average 3x smaller than that of idealized selective coil.

### 7.2 Comparison with MagMIMO

MultiSpot is inspired by MagMIMO [1], which proposes magnetic beamforming to a single device. Thus, in this experiment we compare MagMIMO with MultiSpot. We separate this experiment from the other baselines since MagMIMO is not intended for charging multiple devices. Still one might wonder how MagMIMO would perform when there are multiple devices around, and how does it compare to MultiSpot.

We use the same hardware to run MultiSpot and MagMIMO. We use two receivers and run both MagMIMO and MultiSpot in three different scenarios. In the first scenario, the two receivers are co-located within 5cm from each other, and both are 25cm away from the transmitter. In the second scenario, the receivers are 60cm apart, and both 10cm away from the transmitter. In the third scenario, the two receivers are 60cm apart and both 20cm away from the transmitter.

Fig. 6 shows that MagMIMO is comparable to MultiSpot only when the two phones are co-located and hence can be considered as one device. Otherwise, MagMIMO's charging time becomes an order of magnitude longer than MultiSpot, or it fails to charge one of the phones all together. The reason is that MagMIMO has no mechanism for separating the magnetic couplings of the two receivers, and hence interprets the magnetic channels of both receivers as one channel and tries to create one beam to charge both phones. When the phones are adjacent, this technique works because one beam can charge both receivers, but as this distance increases, the charging time ratio inevitably goes up. MultiSpot on the other hand, creates two beams for both receivers and is able to power both phones regardless of the distance between them.

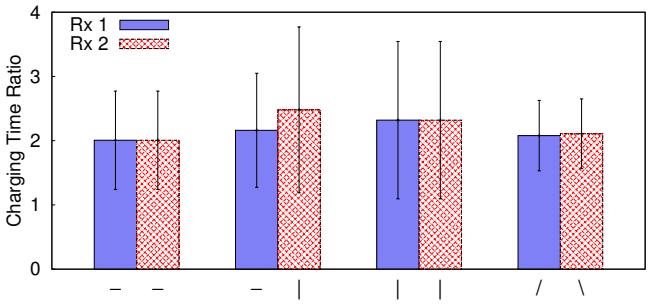


Figure 7: **Charging Time vs. Orientation.** We plot the charging time ratio versus different orientations. Each group of two bars represent a combination of orientations, where "−" denotes horizontal, "|" denotes vertical, while "/" and "\" denote 45°. All receivers are 25cm away from the charger.

### 7.3 Charging Time vs. Orientation

We investigate MultiSpot's performance with different receiver orientations. For all experiments, the distances of both receivers is fixed to be 25cm, while their orientations are varied. We test four scenarios: both phones horizontal, one horizontal and one vertical, both vertical, and both at 45° tilt.

The results in Fig. 7 show that the time that MultiSpot's performance is almost orientation agnostic. Although there are some variations in the charging time ratio between different orientation scenarios, but the difference remain relatively small. For example, charging two horizontal phones take about 2x wired charging time, while two vertical phones take 2.3x wired charging time.

### 7.4 Performance vs. Number of Receivers

Next, we evaluate MultiSpot's performance along a few dimensions as the number of receivers increases.

**Charging Time vs. Number of Receivers:** We evaluate MultiSpot's ability to charge different numbers of receivers. We run

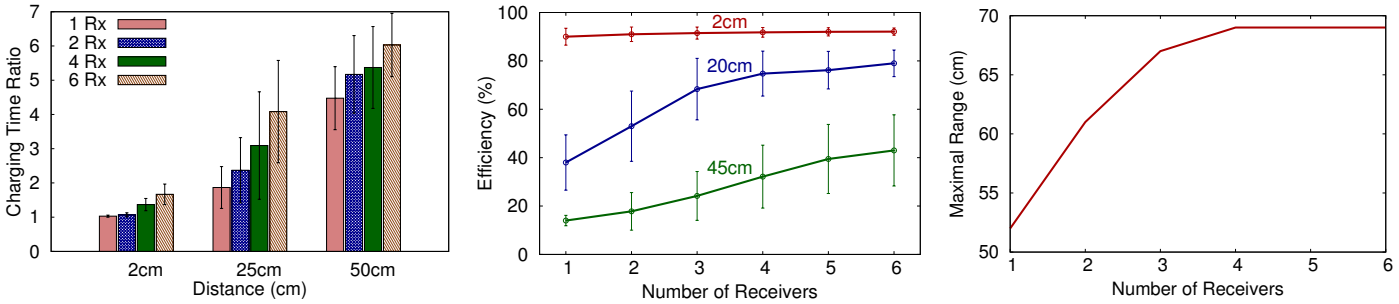


(a) Charging Time Ratio vs. Number of Rx (b) Efficiency vs. Number of Rx (c) Maximal Range vs. Number of Rx

Figure 8: **MultiSpot's Performance with Number of Receivers.** (a) MultiSpot's charging time ratio with up to 6 receivers; (b) MultiSpot's efficiency as a function of receiver number and distance to the charger. (c) MultiSpot's maximal charging range increases with receivers.

experiments with 1, 2, 4, and 6 receivers. In each experiment, all of the receivers are placed at the same distance from the charger, but at random positions and orientations. To show the results we pick three representative distances, 2cm (near range), 25cm (mid range) and 50cm (far range). Fig. 8a shows the charging time ratio versus number of receivers. In all cases MultiSpot is able to charge all of the phones. However, the charging time increases with distance and number of receivers. This is because MultiSpot needs to split more beams when there are more receivers, so the power that is carried in each beam will go down with more receivers.

**Efficiency vs. Number of Receivers:** We test MultiSpot's efficiency with different locations and number of receivers. The distance of all receivers to the transmitter is fixed while the number of receivers is increased. For a given distance and number of receivers, the positions and orientations are varied across runs. We evaluate MultiSpot's efficiency. Similar to past work [1], we define efficiency as the ratio between the total received power at all receiving coils divided by the total input power at the transmitting coils. The experiment is repeated with 3 different distances: near range (2cm), mid range (25cm) and far range (45cm). For each range we repeat the experiments for different number of receivers.

Based on Fig. 8b, we make a few observations:

- For a single device, MultiSpot has similar or better efficiency compared with state-of-the-art systems. For example, MagMIMO [1] reports 89% and 34% efficiency with single device at 2cm and 20cm, while MultiSpot's efficiencies are 90% and 38% at 2cm and 20cm, At near range, MultiSpot's efficiency is better than commercial systems. For example, WiTricity WiT-5000 [15] reaches its best efficiency (90%) at 0.6cm, while MultiSpot has 90% efficiency at a larger distance (2cm).
- We also find it interesting that the system efficiency increases with the number of receivers. For example, at 45cm the efficiency increases from 14% with single device to 43% with 6 receivers. This effect is more apparent when the receivers are at mid-range and far-range. The reason is that the more receivers are around, the more magnetic flux can be picked up by the receivers. This happens because the beams are relatively wide, and hence when there are more receivers, they can collectively pick up more energy.

**Maximal Range vs. Number of Receivers:** As the number of receivers increases, the efficiency of MultiSpot increases. With this increased efficiency, it may be possible to charge a receiver at a larger distance when more receivers are in the system. Therefore, this experiment is aimed to find the maximum distance from the transmitter a phone can still charge from, given a number of receivers. To get a feel of how the range increases with number of devices, we put all phones horizontally above the coils and find the maximal $z$ distance. Different phones are aligned and spaced vertically.

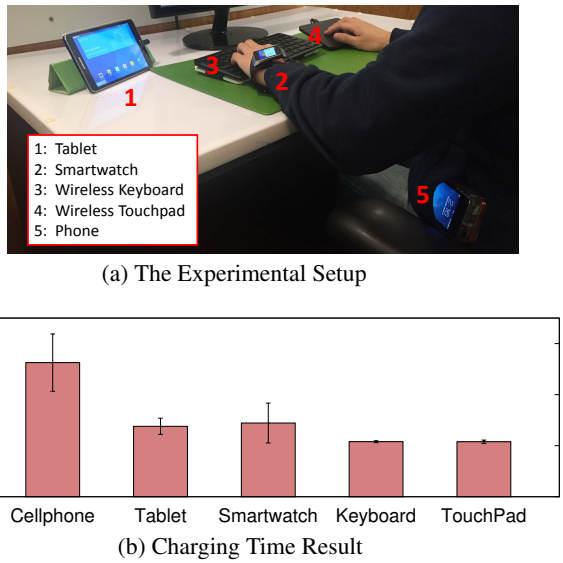


(a) The Experimental Setup

(b) Charging Time Result

Figure 9: **User Experiment:** MultiSpot can charge multiple types of devices concurrently in an office desk scenario as shown in (a).

Fig. 8c shows the maximal charging range vs. the number of receivers. The maximum range does indeed increase with the number of receivers. From one receiver to two receivers, the distance increases by 10cm. With 4 phones, the extension of range is 17cm.

In particular, because of the magnetic coupling between the receivers, one receiver might induce power on another receiver. In this case the receiver acts as a power relay, extending the maximal range of power delivery.

## 7.5 User Experiment

The goal of this experiment is two-fold: first, we want to ensure that MultiSpot works with a diversity of devices; second, we want to show that MultiSpot could charge all devices while the user is interacting with them or moving them.

We use the same setup as used by other experiments. However, we involve a variety of receiver devices. Specifically, we have tested cellphones (iPhone 4s/5s/6, Nexus 4, Samsung Galaxy S4/S5, HTC Evo and Motorola Droid X2), tablets (Samsung Glaxy Tab 4 and Kindle Paper White), smartwatch (Samsung Gear Live Smartwatch), wireless keyboard (Logitech K810) and wireless touchpad

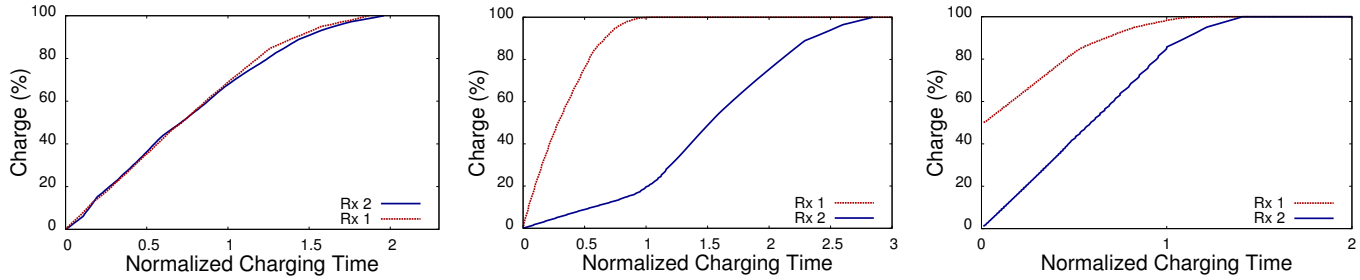


(a) Same Distance and Initial Battery (b) Different Distances (c) Different Initial Battery

Figure 10: **Charging Curves of Two Phones For Three Scenarios:** The x-axis is charge time normalized by charge time of a wall plug to charge from dead battery to full. The scenarios are: (a): Charging two phones from dead batteries, with the same distance (25cm); (b): Same as (a), but with different distances (Rx1: 10cm, Rx2: 40cm). (c): Same as (a) but the two phones start with different battery levels (0%, 50%).

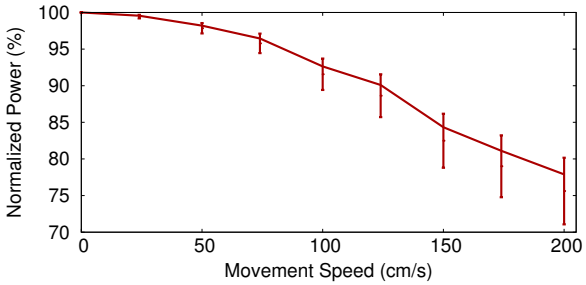


Figure 11: **Normalized Power vs. Motion Speed.** We plot the normalized received power versus different movement speed of the receiver. The reduction of received power is less than 3% when the speed is less than 50cm/s; it goes up to 20%-30% when the receiver moves at 200m/s.

(Logitech T650). In each experiment, we place the keyboard and touchpad flatly on the desk, and place the tablet against a stand. We then ask the user to sit in front of the desk and type on the keyboard, with a cellphone in her pocket and a smartwatch on her wrist (see Fig. 9a for a photo while the experiment is running). We measure the charging time ratio for each type of devices. We repeat the experiment with 3 users.

Fig. 9b shows the charging time ratio of the various device types. MultiSpot can charge all of the devices, however the charging time ratio of each of them is different. The cellphone and smartwatch have relatively higher charging time ratios and standard deviations. This is because they are carried by the user, while the other devices are static on the desk. Also, according to Fig. 9b, the cellphone takes longer than the smartwatch to charge. This is because as the user works, their wrist is moving above the desk while the phone is in their pocket, so naturally the phone is on average farther away from the coils.

Finally, we have used a temperature gun infrared thermometer [43] to monitor the temperature of the devices during the experiment. The maximal temperature increase we have measured is $4^{\circ}$C over a duration of 5 hours.

### 7.6 Power Distribution among Receivers

In this section, we select three representative scenarios to show how MultiSpot distributes power among receivers. We charge two iPhones 5s, in different scenarios:

- *Same Distance and Initial Battery*: We put each of the two phones 25cm away from the charger and let them charge from a dead battery. Fig. 10a shows their charging curve, i.e., battery percentage vs. time. Since all factors of these two phones are almost exactly the same, the phones charge at the same rate, as shown in the figure.
- *Different Distances*: We charge two phones with dead batteries but with different distances from the transmitter (10cm and 40cm). Fig. 10b shows the charging rate of the two phones. The figure shows that initially, the phone closer to the transmitter (i.e., Rx1) charges faster since it has a stronger magnetic coupling with the charger. However, once this phone is fully charged, MultiSpot transfers the power to the second receiver (Rx2), increasing its charging rate. Said differently, when one phone is fully charged and has no demand for power, MultiSpot automatically re-allocates the power to serve the other receiver which still has demands.
- *Different Initial Batteries*: We repeat the previous experiment, with different battery levels (0% and 50%). The results presented in Fig. 10c show that the phone with a lower battery level charges faster. Thus, when all other factors are the same, MultiSpot allocates more power to the device that has a lower battery level, i.e., the device with higher demands for power.

### 7.7 Performance vs. Motion

In this experiment, we aim to evaluate MultiSpot's performance with regard to the motion of the receiver. We use the same setup as other experiments, but add controlled movements to the receiver. Specifically, we attach the receiver to a motor which moves across the table where the charger is mounted, and vary the speeds across different experiments. During the experiments, the receiver is always 15cm above the table.

To measure MultiSpot's performance, we pick 5 evenly distanced locations in the motion's path, measure the received power at each location, and average them. We then normalize it by the power when there is no motion. Fig. 11 shows the normalized power versus motion speed. We can see that MultiSpot works well with mild receiver motion, and degrades if the speed increases. Various surveys [44, 45, 46] have suggested that the average speed of natural human arm movements is under 50cm/s, in which case the received power is almost unaffected (<3% degradation). If the speed reaches 200cm/s, the reduction of power is around 20%-30%.

## 8. Conclusion

This paper presents MultiSpot, a power hotspot that can charge multiple devices wirelessly and simultaneously, at distances up to 50cm. MultiSpot can be attached to an office desk, and used to charge surrounding electronic devices. It can also charge devices carried by the user once she is in the vicinity of a MultiSpot charger. This allows MultiSpot to be used in more practical scenarios, where the area of movement by the user is relatively constrained, such as

bed-stands, car seats, coffee shops, airports waiting seats, etc. We believe MultiSpot pushes the state-of-the-art of wireless charging and significantly improves the user experience. Important tasks for future work include evaluating our system for a wider range of mobile devices and applications, and allowing the system to explicitly specify how much power is delivered to each receiver.

## 9. ACKNOWLEDGEMENTS

We thank the anonymous reviewers and shepherd for their constructive comments. We are grateful to Omid Abari, Fadel Adib, Haitham Hassanieh, Swarun Kumar, John MacDonald, Deepak Vasisht, for their constructive feedbacks. We also thank the NETMIT group for their support. This research is funded by NSF. We thank members of the MIT Wireless Center: Amazon, Cisco, Google, Intel, Mediatek, Microsoft and Telefonica for their interest and general support.

# APPENDIX

## A. PROOF OF THEOREM 4.1

Proof: We start with converting the optimization problem to another equivalent one. Specifically, if we define $\vec{\boldsymbol{x}} = \sqrt{\boldsymbol{R}_T}\vec{\boldsymbol{i}}_T$, [8] then the problem becomes that we want to find $\vec{\boldsymbol{i}}_T^{\text{bf}} = \sqrt{\boldsymbol{R}_T^{-1}}\vec{\boldsymbol{x}}_T^{\text{bf}}$, where $\vec{\boldsymbol{x}}_T^{\text{bf}}$ is the solution to the following:

$$\vec{\boldsymbol{x}}_T^{\text{bf}} = \arg\max_{\vec{\boldsymbol{x}}} \{\vec{\boldsymbol{x}}^* \boldsymbol{A} \vec{\boldsymbol{x}}\}, \text{ where } \boldsymbol{A} \triangleq \sqrt{\boldsymbol{R}_T^{-1}}\boldsymbol{H}^*\boldsymbol{R}_R\boldsymbol{H}\sqrt{\boldsymbol{R}_T^{-1}}$$

The constraint correspondingly becomes $\vec{\boldsymbol{x}}^*\vec{\boldsymbol{x}} + \vec{\boldsymbol{x}}^*\boldsymbol{A}\vec{\boldsymbol{x}} = P$. Now, since $\boldsymbol{A}$ is a positive semi-definite Hermitian matrix (recall both $\boldsymbol{R}_R$ and $\boldsymbol{R}_T$ are real positive diagonal matrices), it can be eigen-decomposed to $\boldsymbol{A} = \boldsymbol{Q}\boldsymbol{\Lambda}\boldsymbol{Q}^*$, where $\boldsymbol{Q}$ is a unitary matrix and $\boldsymbol{\Lambda}$ is a diagonal matrix of the eigenvalues of $\boldsymbol{A}$. Furthermore, all eigenvalues, $\lambda_1, \cdots, \lambda_n$, are real and non-negative. If we define $\vec{\boldsymbol{x}}' = \boldsymbol{Q}^*\vec{\boldsymbol{x}}$, then the objective function $\vec{\boldsymbol{x}}^*\boldsymbol{A}\vec{\boldsymbol{x}}$ can be written as $\left(\vec{\boldsymbol{x}}'\right)^*\boldsymbol{\Lambda}\vec{\boldsymbol{x}}' = \sum_i \lambda_i |x_i'|^2$. Similarly, the constraint becomes: $\vec{\boldsymbol{x}}^*\vec{\boldsymbol{x}} + \vec{\boldsymbol{x}}^*\boldsymbol{A}\vec{\boldsymbol{x}} = \left(\vec{\boldsymbol{x}}'\right)^*\vec{\boldsymbol{x}}' + \left(\vec{\boldsymbol{x}}'\right)^*\boldsymbol{\Lambda}\vec{\boldsymbol{x}}' = \sum_i(\lambda_i+1)|x_i'|^2$. Therefore, we have converted our optimization problem to:

$$\begin{array}{ll} \max & \sum_i \lambda_i |x_i'|^2 \\ \text{s.t.} & \sum_i (\lambda_i+1)|x_i'|^2 = P \end{array}$$

Since all $\lambda_i$'s are real non-negative, the optimal solution $\vec{\boldsymbol{x}}'$ is zero in every entry except the one that $\lambda_i$ is maximal. More formally, say that $\lambda_k = \arg\max\{\lambda_1, \cdots, \lambda_n\}$, then $\vec{\boldsymbol{x}}'$ is zero on entries except the $k$-th one. In this case, the maximal value that is achieved is $\frac{\lambda_k}{\lambda_k+1}P$. Recall that $\vec{\boldsymbol{x}}' = \boldsymbol{Q}^*\vec{\boldsymbol{x}}$, or equivalently, $\vec{\boldsymbol{x}} = \boldsymbol{Q}\vec{\boldsymbol{x}}'$. Therefore, the optimal solution $\vec{\boldsymbol{x}}_T^{\text{bf}}$ is proportional to $k$-th column of $\boldsymbol{Q}$ (i.e., the $k$-th eigenvector of $\boldsymbol{A}$). Substituting back $\vec{\boldsymbol{x}} = \sqrt{\boldsymbol{R}_T}\vec{\boldsymbol{i}}_T$, we get the optimal $\vec{\boldsymbol{i}}_T^{\text{bf}}$:

$$\vec{\boldsymbol{i}}_T^{\text{bf}} = c \cdot \sqrt{\boldsymbol{R}_T^{-1}} \cdot \text{maxeig}\left(\sqrt{\boldsymbol{R}_T^{-1}}\boldsymbol{H}^*\boldsymbol{R}_R\boldsymbol{H}\sqrt{\boldsymbol{R}_T^{-1}}\right)$$

In this paper, to simplify the equations, we assume the transmitter coils are identical, i.e., $R_{T1} = \cdots = R_{Tn} = R_T$. In this case, $\boldsymbol{R}_T$ is proportional to an identity matrix, thus when multiplied with another matrix, will not change it eigenvectors. Therefore, in this case, the solution is $\vec{\boldsymbol{i}}_T^{\text{bf}} = c \cdot \text{maxeig}(\boldsymbol{H}^*\boldsymbol{R}_R\boldsymbol{H})$. $c$ is a scalar that captures $R_T$ and other terms. It can be solved by substituting $\vec{\boldsymbol{i}}_T$ by $\vec{\boldsymbol{i}}_T^{\text{bf}}$ to the constraint $\vec{\boldsymbol{i}}_T^*\boldsymbol{R}_T\vec{\boldsymbol{i}}_T + \vec{\boldsymbol{i}}_T^*\boldsymbol{H}^*\boldsymbol{R}_R\boldsymbol{H}\vec{\boldsymbol{i}}_T = P$. Note that this does not substantially change any of the conclusions in this paper; plugging back $\boldsymbol{R}_T$ into them is straightforward.

[8] $\sqrt{\boldsymbol{R}_T}$ is a diagonal matrix whose diagonal entries are square root of those of $\boldsymbol{R}_T$. Similarly, $\sqrt{\boldsymbol{R}_R}$ can be defined.

## B. PROOF OF THEOREM 4.2

Let's first expand $\boldsymbol{H}^*\boldsymbol{R}_R\boldsymbol{H}$ and $\boldsymbol{Y}$: $\boldsymbol{H}^*\boldsymbol{R}_R\boldsymbol{H} = \omega^2\boldsymbol{M}^\top\left(\boldsymbol{Z}_R^{-1}\right)^*\boldsymbol{R}_R\boldsymbol{Z}_R^{-1}\boldsymbol{M}$, and $\boldsymbol{Y} = \omega^2\boldsymbol{M}^\top\boldsymbol{Z}_R^{-1}\boldsymbol{M}$. Recall that $\boldsymbol{M}$ is a real matrix, therefore in order to prove $\boldsymbol{H}^*\boldsymbol{R}_R\boldsymbol{H} = \text{Real}(\boldsymbol{Y})$, what we need to prove is

$$\left(\boldsymbol{Z}_R^{-1}\right)^*\boldsymbol{R}_R\boldsymbol{Z}_R^{-1} = \text{Real}\left(\boldsymbol{Z}_R^{-1}\right)$$

which is proved as follows:

Proof: Note that: 1) $\boldsymbol{R}_R$ is the real part of $\boldsymbol{Z}_R$, therefore,

$$\boldsymbol{R}_R = \frac{1}{2}\left(\boldsymbol{Z}_R + \overline{\boldsymbol{Z}_R}\right) \tag{15}$$

where $\overline{\boldsymbol{Z}_R}$ means entry-wise conjugate of $\boldsymbol{Z}_R$; 2) $\boldsymbol{Z}_R$ is symmetric, i.e., $\boldsymbol{Z}_R = \boldsymbol{Z}_R^\top$, thus by conjugating both sides, we get $\overline{\boldsymbol{Z}_R} = \boldsymbol{Z}_R^*$. Inverting both sides yields

$$\left(\overline{\boldsymbol{Z}_R}\right)^{-1} = \left(\boldsymbol{Z}_R^{-1}\right)^* \tag{16}$$

Substituting them, we get:

$$\begin{aligned} \left(\boldsymbol{Z}_R^{-1}\right)^*\boldsymbol{R}_R\boldsymbol{Z}_R^{-1} &\overset{\text{Eq. (15)}}{\Longrightarrow} \frac{1}{2}\left(\boldsymbol{Z}_R^{-1}\right)^*\left(\boldsymbol{Z}_R + \overline{\boldsymbol{Z}_R}\right)\boldsymbol{Z}_R^{-1} \\ &\overset{\text{Eq. (16)}}{\Longrightarrow} \frac{1}{2}\left(\boldsymbol{Z}_R^{-1}\right)^* + \frac{1}{2}\left(\overline{\boldsymbol{Z}_R}\right)^{-1}\overline{\boldsymbol{Z}_R}\boldsymbol{Z}_R^{-1} \\ &\overset{\text{Eq. (16)}}{\Longrightarrow} \frac{1}{2}\left(\overline{\boldsymbol{Z}_R^{-1}} + \boldsymbol{Z}_R^{-1}\right) = \text{Real}\left(\boldsymbol{Z}_R^{-1}\right) \end{aligned}$$

Thus, $\left(\boldsymbol{Z}_R^{-1}\right)^*\boldsymbol{R}_R\boldsymbol{Z}_R^{-1} = \text{Real}\left(\boldsymbol{Z}_R^{-1}\right)$. □

## C. PROOF OF THEOREM 4.3

We prove the theorem by showing that the rank of $\boldsymbol{Y} - \widetilde{\boldsymbol{Y}}$ gets reduced in every iteration, by the following lemma:

LEMMA C.1. *For any complex symmetric matrix $\boldsymbol{A}$ (i.e., $\boldsymbol{A} = \boldsymbol{A}^\top$), any vector $\vec{\boldsymbol{\eta}}$ such that $\vec{\boldsymbol{\eta}}^\top\boldsymbol{A}\vec{\boldsymbol{\eta}} \neq 0$, define $\vec{\boldsymbol{\xi}} = \boldsymbol{A}\vec{\boldsymbol{\eta}}$, then rank $\left(\boldsymbol{A} - \frac{\vec{\boldsymbol{\xi}}\vec{\boldsymbol{\xi}}^\top}{\vec{\boldsymbol{\xi}}^\top\vec{\boldsymbol{\eta}}}\right) \leq$ rank$(\boldsymbol{A}) - 1$.*

Proof: Since $\boldsymbol{A}$ is a complex symmetric matrix, there exists an Autonne-Takagi factorization [47] such that

$$\boldsymbol{A} = \boldsymbol{Q}\boldsymbol{\Lambda}\boldsymbol{Q}^\top, \text{ where } \boldsymbol{\Lambda} = \begin{bmatrix} \boldsymbol{\Lambda}_0 & \boldsymbol{O} \\ \boldsymbol{O} & \boldsymbol{O} \end{bmatrix}$$

where $\boldsymbol{Q}$ is a $n \times n$ unitary matrix, and $\boldsymbol{\Lambda}_0$ is a $r \times r$ diagonal matrix, where $r$ is the rank of $\boldsymbol{A}$. Now substitute this as well as $\vec{\boldsymbol{\xi}} = \boldsymbol{A}\vec{\boldsymbol{\eta}}$, we get:

$$\boldsymbol{A} - \frac{\vec{\boldsymbol{\xi}}\vec{\boldsymbol{\xi}}^\top}{\vec{\boldsymbol{\xi}}^\top\vec{\boldsymbol{\eta}}} = \boldsymbol{Q}\left(\boldsymbol{\Lambda} - \frac{\boldsymbol{\Lambda}\boldsymbol{Q}^\top\vec{\boldsymbol{\eta}}\vec{\boldsymbol{\eta}}^\top\boldsymbol{Q}\boldsymbol{\Lambda}}{\vec{\boldsymbol{\eta}}^\top\boldsymbol{Q}\boldsymbol{\Lambda}\boldsymbol{Q}^\top\vec{\boldsymbol{\eta}}}\right)\boldsymbol{Q}^\top \tag{17}$$

Define $\vec{\boldsymbol{\zeta}} = \boldsymbol{Q}^\top\vec{\boldsymbol{\eta}}$, and substitute it into Eq. (17), we get

$$\boldsymbol{A} - \frac{\vec{\boldsymbol{\xi}}\vec{\boldsymbol{\xi}}^\top}{\vec{\boldsymbol{\xi}}^\top\vec{\boldsymbol{\eta}}} = \boldsymbol{Q}\begin{bmatrix} \boldsymbol{\Lambda}_0 - \frac{\boldsymbol{\Lambda}_0\vec{\boldsymbol{\zeta}}_0\vec{\boldsymbol{\zeta}}_0^\top\boldsymbol{\Lambda}_0}{\vec{\boldsymbol{\zeta}}_0^\top\boldsymbol{\Lambda}_0\vec{\boldsymbol{\zeta}}_0} & \vec{\boldsymbol{0}} \\ \vec{\boldsymbol{0}}^\top & \boldsymbol{O} \end{bmatrix}\boldsymbol{Q}^\top$$

Since $\boldsymbol{Q}$ is unitary, the rank of $\boldsymbol{A} - \frac{\vec{\boldsymbol{\xi}}\vec{\boldsymbol{\xi}}^\top}{\vec{\boldsymbol{\xi}}^\top\vec{\boldsymbol{\eta}}}$ is equal to the rank of $\boldsymbol{\Lambda}_0 - \frac{\boldsymbol{\Lambda}_0\vec{\boldsymbol{\zeta}}_0\vec{\boldsymbol{\zeta}}_0^\top\boldsymbol{\Lambda}_0}{\vec{\boldsymbol{\zeta}}_0^\top\boldsymbol{\Lambda}_0\vec{\boldsymbol{\zeta}}_0}$, which we define as matrix $\boldsymbol{B}$. If we define $\vec{\boldsymbol{\zeta}}_0$ to be the first $r$ entries of $\vec{\boldsymbol{\zeta}}$, we observe that:

$$\boldsymbol{B}\vec{\boldsymbol{\zeta}}_0 = \boldsymbol{\Lambda}_0\vec{\boldsymbol{\zeta}}_0 - \frac{\boldsymbol{\Lambda}_0\vec{\boldsymbol{\zeta}}_0\vec{\boldsymbol{\zeta}}_0^\top\boldsymbol{\Lambda}_0}{\vec{\boldsymbol{\zeta}}_0^\top\boldsymbol{\Lambda}_0\vec{\boldsymbol{\zeta}}_0}\vec{\boldsymbol{\zeta}}_0 = \boldsymbol{\Lambda}_0\vec{\boldsymbol{\zeta}}_0 - \boldsymbol{\Lambda}_0\vec{\boldsymbol{\zeta}}_0 = \vec{\boldsymbol{0}}$$

i.e., $\boldsymbol{B}$ is not full rank, such that rank$(\boldsymbol{B}) \leq$ rank$(\boldsymbol{A}) - 1$. Therefore, rank $\left(\boldsymbol{A} - \frac{\vec{\boldsymbol{\xi}}\vec{\boldsymbol{\xi}}^\top}{\vec{\boldsymbol{\xi}}^\top\vec{\boldsymbol{\eta}}}\right) \leq$ rank$(\boldsymbol{A}) - 1$. □

Since $\boldsymbol{Y}$ is a complex symmetric matrix, we can set $\boldsymbol{A} = \boldsymbol{Y} - \tilde{\boldsymbol{Y}}$, $\vec{\boldsymbol{\eta}} = \vec{\boldsymbol{i}}_T$, thus $\vec{\boldsymbol{\xi}} = (\boldsymbol{Y} - \tilde{\boldsymbol{Y}})\vec{\boldsymbol{i}}_T = \Delta\vec{\boldsymbol{v}}_T$. Therefore, applying the lemma, we get: rank $\left(\boldsymbol{Y} - \tilde{\boldsymbol{Y}} - \frac{\Delta\vec{\boldsymbol{v}}_T \Delta\vec{\boldsymbol{v}}_T^\top}{\Delta\vec{\boldsymbol{v}}_T^\top \vec{\boldsymbol{i}}_T}\right) \leq \text{rank}(\boldsymbol{Y} - \tilde{\boldsymbol{Y}}) - 1$. This means that the rank of $\boldsymbol{Y} - \tilde{\boldsymbol{Y}}$ gets reduced by at least 1 in each iteration. Since the initial rank cannot be larger than $n$, which is the size of the matrix, then the number of iterations that is needed cannot exceed $n$.

## D. PRE-CALIBRATION

The goal of pre-calibration is to estimate $\boldsymbol{Z}_T$. It can be done immediately after manufacturing the transmitter coils where their relative positions are hardcoded. During pre-calibration, there is no receiver around, so the Transmitter Eq. (6) is reduced to $\vec{\boldsymbol{v}}_T = \boldsymbol{Z}_T\vec{\boldsymbol{i}}_T$. Now, in order to estimate $\boldsymbol{Z}_T$, we need to apply $n$ different sets of $\vec{\boldsymbol{v}}_T$ and measure the corresponding $\vec{\boldsymbol{i}}_T$. $\boldsymbol{Z}_T$ can be consequently obtained by matrix inversion, i.e., similar to how we estimate $\boldsymbol{Y}$ in Sec. §4.2.

## 10. REFERENCES


[1] J. Jadidian and D. Katabi. Magnetic MIMO: How to charge your phone in your pocket. In *ACM MobiCom*, 2014.

[2] A. Sample, B. Waters, S. Wisdom, and J. Smith. Enabling seamless wireless power delivery in dynamic environments. *Proceedings of the IEEE*, 101(6), 2013.

[3] Datasheet for Qi-enabled charger. RAV Power.

[4] Duracell powermat for 2 devices. Duracell Corp.

[5] Energizer dual inductive charger. Energizer.

[6] Qi specification 1.1.2, 2014. Wireless Power Consortium.

[7] Rezence specification. Alliance for Wireless Power.

[8] Highly resonant wireless power transfer: Safe, efficient, and over distance. Technical report, WiTricity Corp, 2012.

[9] Wattup. Energous Corp.

[10] Cota wireless power. Ossia Inc.

[11] Wireless charging, at a distance, moves forward for ubeam, 2014. The New York Times.

[12] Wi-charge. http://www.wi-charge.com/about.php.

[13] F. C. Delori, R. H. Webb, and D. H. Sliney. Maximum permissible exposures for ocular safety (ansi 2000), with emphasis on ophthalmic devices. 2007.

[14] M. Zahn. *Electromagnetic Field Theory: A Problem Solving Approach*. Krieger Pub Co, 2003.

[15] WiT-5000 development kit data sheet. WiTricity Corporation.

[16] TX-200 dual wireless charging pad. LUXA2.

[17] Nokia wireless charging plate. Nokia Corp.

[18] J. Cassell. http://press.ihs.com/press-release/technology/apple-watch-spurs-rapid-growth-market-wireless-charging-wearable-technology.

[19] P. Li and R. Bashirullah. A wireless power interface for rechargeable battery operated medical implants. *Circuits and Systems II, IEEE Transactions on*, 2007.

[20] S. Kim, J. S. Ho, and A. S. Poon. Wireless power transfer to miniature implants: Transmitter optimization. *Antennas and Propagation, IEEE Transactions on*, 2012.

[21] U. K. Madawala and D. J. Thrimawithana. A bidirectional inductive power interface for electric vehicles in V2G systems. *Industrial Electronics, IEEE Transactions on*, 2011.

[22] B. Tong, Z. Li, G. Wang, and W. Zhang. How wireless power charging technology affects sensor network deployment and routing. In *Distributed Computing Systems, IEEE*, 2010.

[23] L. Xie, Y. Shi, Y. T. Hou, and A. Lou. Wireless power transfer and applications to sensor networks. *Wireless Communications, IEEE*, 2013.

[24] Proxi-point transmitter for the LTC4120. PowerByProxi.

[25] A. Kurs, A. Karalis, R. Moffatt, J. D. Joannopoulos, P. Fisher, and M. Soljačić. Wireless power transfer via strongly coupled magnetic resonances. 317(5834), 2007.

[26] B. L. Cannon, J. F. Hoburg, D. D. Stancil, and S. C. Goldstein. Magnetic resonant coupling as a potential means for wireless power transfer to multiple small receivers. *Power Electronics, IEEE Transactions on*, 2009.

[27] J. Casanova, Z. N. Low, and J. Lin. A loosely coupled planar wireless power system for multiple receivers. *Industrial Electronics, IEEE Transactions on*, 56(8), 2009.

[28] J. Kim, D. Kim, and Y. Park. Analysis of capacitive impedance matching networks for simultaneous wireless power transfer to multiple devices. *Industrial Electronics, IEEE Transactions on*, 2014.

[29] J.-W. Kim, H.-C. Son, D.-H. Kim, K.-H. Kim, and Y.-J. Park. Analysis of wireless energy transfer to multiple devices using cmt. In *Microwave Conference Proceedings, IEEE*, 2010.

[30] D. Ahn and S. Hong. Effect of coupling between multiple transmitters or multiple receivers on wireless power transfer. *Industrial Electronics, IEEE Transactions on*, 60(7), 2013.

[31] A. Kurs, R. Moffatt, and M. Soljacić. Simultaneous mid-range power transfer to multiple devices. *Applied Physics Letters*, 2010.

[32] D. Ahn and S. Hong. A study on magnetic field repeater in wireless power transfer. *Industrial Electronics, IEEE Transactions on*, 2013.

[33] B. Waters, B. Mahoney, V. Ranganathan, and J. Smith. Power delivery and leakage field control using an adaptive phased-array wireless power system. *(Accepted and Pre-Published) IEEE Transactions on Power Electronics*.

[34] M. Moon. uBeam demo video. http://www.engadget.com/2014/08/07/ubeam-wireless-charger-ultrasound/.

[35] S. Budiansky. *Truth about Dogs*. 2000.

[36] Performance standards for microwave and radio frequency emitting products. Title 21, Part 1030, U.S. Food and Drug Administration.

[37] W. H. Paul Horowitz. *The Art of Electronics*. Cambridge University Press, 1989.

[38] Understanding li+ battery operation lessens charging safety concerns. Technical Report APP 4169, Maxim Integrated Products, Inc., 2008.

[39] Can witricity technology transfer power through walls or obstructions? http://witricity.com/technology/witricity-faqs/.

[40] AD8333: DC to 50 MHz, dual I/Q demodulator and phase shifter data sheet (Rev. E). Analog Devices.

[41] Zynq-7000 all programmable soc (z-7010, z-7015, and z-7020): Technical reference manual. Xlin.

[42] M. K. Kazimierczuk. Class d voltage-switching mosfet power amplifier. In *Electric Power Applications, IEEE*, 1991.

[43] Temperature gun infrared thermometers. Omega Inc.

[44] P. Morasso. Spatial control of arm movements. *Experimental Brain Research*, 42(2), 1981.

[45] C. Atkeson and J. Hollerbach. Kinematic features of unrestrained vertical arm movements. *The Journal of Neuroscience*, 5(9), 1985.

[46] W. Abend, E. Bizzi, and P. Morasso. Human arm trajectory formation. *Brain*, 1982.

[47] T. Takagi. On an algebraic problem related to an analytic theorem of Carathéodory and Fejér and on an allied theorem of landau. *Japan. J. Math*, 1, 1924.